A Comparative Study of Linear Surface Geoelectrical Electrode Arrays for Enhanced Depth Sensitivity Analysis

Amir Yazdanpanah[1]
[1] School of Mining Engineering, College of Engineering, University of Tehran, Tehran, Iran.
Amiryazdanpanah13@ut.ac.ir

ABSTRACT

Geoelectrical surveys are essential for investigating subsurface electrical resistivity distributions, with electrode array configurations significantly influencing depth sensitivity and resolution. This study compares the performance of six electrode arrays—Wenner Alpha, Schlumberger, Dipole-Dipole, Wenner Beta, Pole-Dipole, and Pole-Pole—in resolving subsurface resistivity variations. Using numerical simulations with a synthetic subsurface model featuring a layered structure and a high-resistivity anomaly, the sensitivity patterns, apparent resistivity distributions, and inverted resistivity models of these arrays are analyzed. Results reveal distinct trade-offs in depth penetration, lateral resolution, and signal-to-noise ratio, with Wenner Alpha and Schlumberger providing robust depth sensitivity for shallow to intermediate depths, while Dipole-Dipole and Pole-Dipole excel in deeper investigations. Pole-Pole arrays offer broad sensitivity but lower resolution, suitable for large-scale surveys. These findings guide the selection of optimal electrode configurations for specific geoelectrical survey objectives.

Keywords: *Electrode arrays, Sensitivity, Electrical Resistivity, Depth, Resolution.*

1. *INTRODUCTION*

Geoelectrical methods, such as electrical resistivity tomography (ERT) and induced polarization (IP), are cornerstone techniques in geophysical exploration, enabling non-invasive characterization of subsurface properties [1]. ERT measures the resistance of subsurface materials to electrical current flow, providing insights into geological structures, lithology, and fluid content. IP quantifies the charge storage capacity of materials, useful for identifying metallic minerals, clay content, and hydrogeological properties. These methods are applied in mineral exploration, groundwater mapping, environmental monitoring, and geotechnical investigations. By injecting current and measuring potential differences, geoelectrical surveys reveal subsurface heterogeneities, making them essential for understanding complex geological systems.

The performance of electrode arrays in geoelectrical surveys has been extensively studied, highlighting their impact on data quality and subsurface resolution [2], [3]. Wenner Alpha, Schlumberger, Dipole-Dipole, and Pole-Dipole arrays are commonly used due to their balanced depth sensitivity and resolution, while Wenner Beta and Pole-Pole arrays are less frequent but valuable for specific applications [4]. Studies have shown that arrays like Wenner Alpha offer high signal-to-noise ratios, whereas Pole-Pole arrays achieve greater depth penetration at the cost of resolution [5]. Comparative analyses emphasize the trade-offs between depth of investigation and vertical resolution, guiding array selection for diverse geophysical objectives [6].

The choice of electrode array configuration in geoelectrical surveys significantly influences data quality and interpretability [2]. The six arrays evaluated in this study—Wenner Alpha, Schlumberger, Dipole-Dipole, Wenner Beta, Pole-Dipole, and Pole-Pole—exhibit unique sensitivity patterns that affect their ability to resolve subsurface features [5]. Some arrays prioritize deep penetration, suitable for thick sedimentary layers, while others excel in delineating lateral variations, ideal for detecting faults or localized anomalies [4]. The selection of an appropriate array depends on survey objectives, such as mapping layered stratigraphy or identifying narrow mineral veins. Inappropriate array selection can lead to poor resolution or misinterpretation, underscoring the need for comparative analysis [6].

Depth sensitivity, governed by electrode geometry, determines an array's ability to detect subsurface features at varying depths [3]. Larger electrode spacings probe deeper but may reduce lateral resolution, while compact configurations enhance near-surface detail but limit depth penetration [7]. Accurate depth sensitivity is critical for applications like aquifer characterization or archaeological surveys, where precise delineation of shallow or deep features is required.

The signal-to-noise ratio (SNR) also impacts data quality (Dahlin & Zhou, 2004). Arrays like Wenner Alpha, with closely spaced potential electrodes, often yield higher SNR due to stronger potential signals, making them suitable for noisy environments. Conversely, Pole-Pole arrays, with widely separated electrodes, may have lower SNR but offer greater depth penetration. Understanding SNR variations enables optimization of survey designs for specific field conditions, balancing resolution, depth sensitivity, and data reliability (White et al., 2003).

2. METHODOLOGY

This study employs numerical simulations using the pyGIMLi [9] geophysical modeling package to evaluate the depth sensitivity and performance of six electrode arrays: Wenner Alpha, Schlumberger, Dipole-Dipole, Wenner Beta, Pole-Dipole, and Pole-Pole. A synthetic subsurface model, featuring a layered structure with a high-resistivity anomaly, is constructed to enable controlled comparison of array performance. The model domain spans from -10 m to 20 m horizontally and from 0 m to -10 m vertically, discretized into a 2D mesh to capture both shallow and deep features.

The apparent resistivity, denoted ρ_a, is calculated for each array configuration using the equation:

$$\rho_a = k\frac{\Delta V}{I} \tag{1}$$

where ΔV is the potential difference measured between the potential electrodes, I is the injected current, and k is the geometric factor determined by the electrode arrangement. The geometric factor k accounts for the spatial configuration of the current (A, B) and potential (M, N) electrodes and is given by [10]:

$$k = 2\pi\left(\frac{1}{\mathrm{AM}} - \frac{1}{\mathrm{BM}} - \frac{1}{\mathrm{AN}} + \frac{1}{\mathrm{BN}}\right)^{-1} \tag{2}$$

Where AM, BM, AN, and BN represent the distances between the respective electrodes (e.g., AM is the distance between the current electrode A and potential electrode M). This general form of k applies to all four-electrode arrays and varies depending on the specific geometry of each configuration.

A 2D mesh is generated to discretize the subsurface model, ensuring sufficient resolution to capture both shallow and deep features. Each electrode array is simulated with identical electrode positions along a linear profile, with configurations defined to reflect their typical field setups. For example, Wenner Alpha uses equal spacing between electrodes, while Dipole-Dipole employs separated current and potential dipoles. The sensitivity of each array is analyzed by computing the Jacobian matrix, which maps the contribution of subsurface resistivity variations to the measured potential differences. Sensitivity distributions are normalized to facilitate direct comparison across arrays, focusing on their ability to resolve depth-dependent resistivity contrasts. The signal-to-noise ratio (SNR) is also evaluated by introducing a fixed error level to the simulated data, allowing assessment of each array's robustness under noisy conditions. The results are visualized as sensitivity maps and inverted resistivity models to compare depth penetration, lateral resolution, and data quality across the arrays.

The sensitivity distributions illustrated in Figures 1–6 are derived from the Jacobian matrix, which quantifies the influence of subsurface resistivity variations on the measured potential differences for each electrode configuration of the six arrays (Wenner Alpha, Wenner Beta, Schlumberger, Dipole-Dipole, Pole-Dipole, and Pole-Pole). The following equations define the sensitivity and its normalized form, used to visualize the subsurface regions most affecting the measurements, as detailed in Table 1.

$$S_{ij} = \frac{\partial(\Delta V_i)}{\Delta \rho_j} \quad (3)$$

$$S_{norm,j} = \frac{S_j / V_j}{\max\left(\left| S_j / V_j \right|\right)} \quad (4)$$

The parameters in the equations include S_{ij}, which represents the sensitivity of the i-th measurement to the j-th subsurface cell's resistivity, and ΔV_i, the potential difference measured between the potential electrodes for the i-th configuration. The term ρ_j denotes the resistivity of the j-th cell in the model mesh, while V_j indicates the volume (or area in 2D) of that cell. The normalized sensitivity, $S_{norm,j}$, scales the sensitivity relative to its maximum value after adjusting for cell size, facilitating comparison across different electrode configurations.

In the final stage, inversion is performed to reconstruct subsurface resistivity models from the apparent resistivity data for each array. The inversion process employs a least-squares optimization technique, incorporating the 3% error model to stabilize the solution, and produces the resistivity distributions shown in Figure 10. These inverted models enable a comparative analysis of each array's performance in resolving the synthetic model's layered structure and high-resistivity anomaly, focusing on depth penetration, lateral resolution, and data quality.

3. GEOELECTRICAL SIMULATION

To evaluate the depth sensitivity and performance of the seven electrode arrays—Wenner Alpha, Schlumberger, Dipole-Dipole, Wenner Beta, Pole-Dipole, and Pole-Pole—a synthetic subsurface model is constructed using the pyGIMLi geophysical modeling package. The model represents a 2D geological environment designed to mimic realistic subsurface conditions, consisting of a layered structure with distinct resistivity zones and an embedded high-resistivity anomaly. Specifically, the model includes a shallow layer with a resistivity of 100 Ωm, representing sandy soil, a deeper layer with a resistivity of 30 Ωm, simulating loam or clay, and a rectangular inclusion with a resistivity of 300 Ωm, resembling a gravel lens. The model domain spans from -10 m to 20 m horizontally and from 0 m to -10 m vertically, with the layers and anomaly strategically placed to test the arrays' ability to resolve both vertical and lateral electrical resistivity contrasts.

The purpose of the simulation is to provide a controlled environment to compare the sensitivity of each electrode array to depth-dependent resistivity variations. By simulating the electrical response of each array over the same subsurface model, the study isolates the effects of array geometry on depth penetration, lateral resolution, and data quality. Electrode positions are defined along a linear profile with a uniform spacing of 1 m, and each array is configured according to its standard field setup. For instance, Wenner Alpha uses equal electrode spacing, while Pole-Dipole employs a single current electrode with a remote pole. The simulated apparent resistivity, ρ_a, is computed for each array, and sensitivity distributions are derived to map how effectively each configuration detects the layered structure and the embedded anomaly. Additionally, a fixed error level of 3% is introduced to the simulated data to assess the signal-to-noise ratio (SNR) under realistic noisy conditions. These simulations enable a quantitative comparison of the arrays' performance, providing insights into their suitability for specific geophysical applications, such as aquifer mapping or mineral exploration, where accurate depth resolution is critical.

4. RESULTS AND DISCUSSION

The geoelectrical simulations compare the depth sensitivity and resolution capabilities of six electrode arrays: Wenner Alpha, Schlumberger, Dipole-Dipole, Wenner Beta, Pole-Dipole, and Pole-Pole, using the synthetic subsurface model described in the Geoelectrical Simulation section. Sensitivity distributions, apparent resistivity, and inverted electrical resistivity models are analyzed to evaluate each array's effectiveness in resolving the subsurface structure, focusing on depth penetration and lateral resolution.

Normalized sensitivity distributions for the Wenner Alpha array, calculated from the Jacobian matrix, map the contribution of subsurface electrical resistivity variations to the measured potential differences, ΔV, as shown in Figure 1. The figure comprises six subplots (a–f), corresponding to distinct four-point electrode configurations with the geometry, characteristic of alpha-type arrays. Each subplot visualizes the sensitivity using a blue-white-red colormap, with blue indicating negative sensitivity, red positive, and white near-zero, highlighting the subsurface regions most influencing the measurements. Current electrodes (A, B) are marked in green, and potential electrodes (M, N) in magenta, to clarify the array geometry. The configurations capture a range of electrode separations, from closely spaced to wider spacings, allowing an assessment of how depth sensitivity and lateral resolution change with array geometry. Smaller electrode spacings emphasize shallow subsurface regions, providing higher resolution near the surface, while larger spacings probe deeper regions, enhancing depth penetration. Wider configurations exhibit broader sensitivity patterns, which improve depth sensitivity but may reduce lateral resolution, whereas compact configurations focus sensitivity closer to the surface, enhancing resolution of near-surface structures.

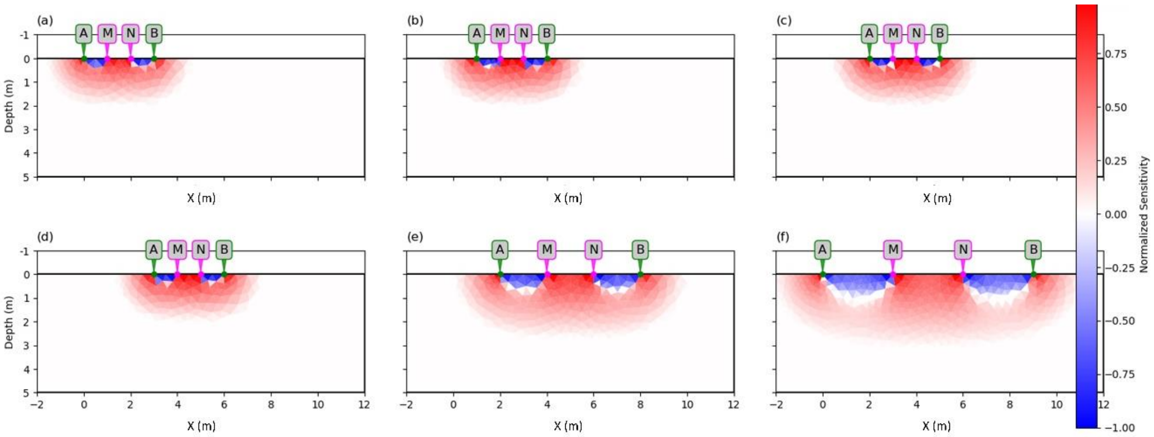

Fig. 1. Plotted Normalized Sensitivity for Wenner-alpha array.

Sensitivity distributions for the Schlumberger array, spanning various electrode separations, are presented in Figure 2, which includes six subplots (a–f), each depicting a distinct four-point electrode configuration, following the geometry of the array. These configurations allow assessment of depth sensitivity and lateral resolution. Narrower separations concentrate sensitivity in shallow subsurface regions, enhancing near-surface resolution, while wider separations extend sensitivity to deeper regions, improving depth penetration but potentially reducing lateral resolution.

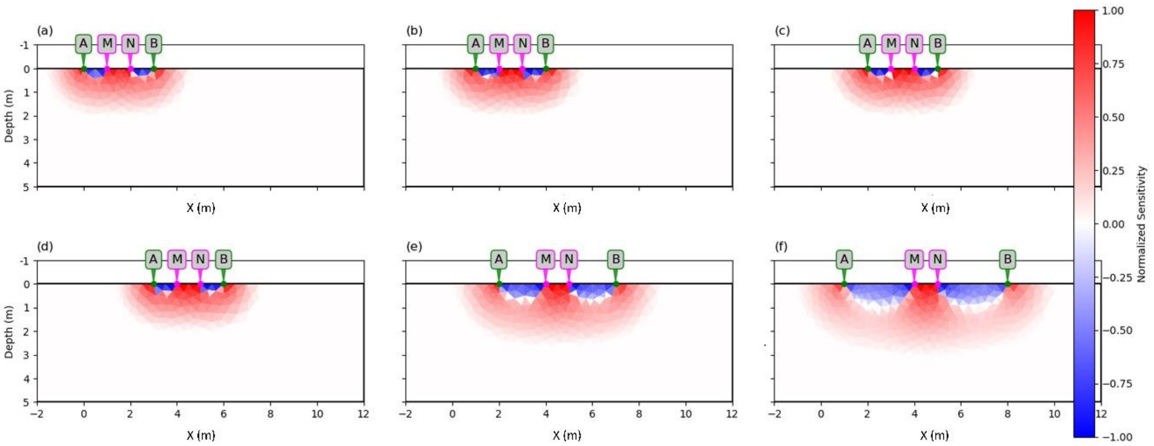

Fig. 2. Plotted Normalized Sensitivity for Schlumberger array**.**

Varying dipole lengths and electrode separations for the Dipole-Dipole array are evaluated through sensitivity distributions shown in Figure 3, featuring six subplots (a–f), each corresponding to a unique four-point electrode configuration, following the geometry of the array. Narrow dipole lengths and smaller separations focus sensitivity in shallow subsurface regions, offering enhanced near-surface resolution, while larger separations and dipole lengths extend sensitivity deeper, improving depth penetration but potentially compromising lateral resolution.

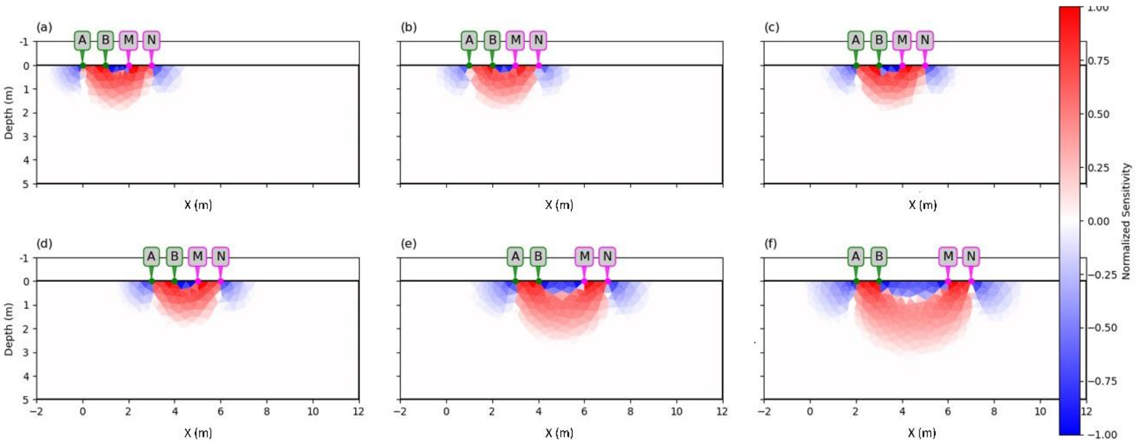

Fig. 3. Plotted Normalized Sensitivity for Dipole-Dipole array**.**

Figure 4 illustrates the sensitivity distributions for the Wenner Beta array, comprising six subplots (a–f), each representing a distinct four-point electrode configuration.

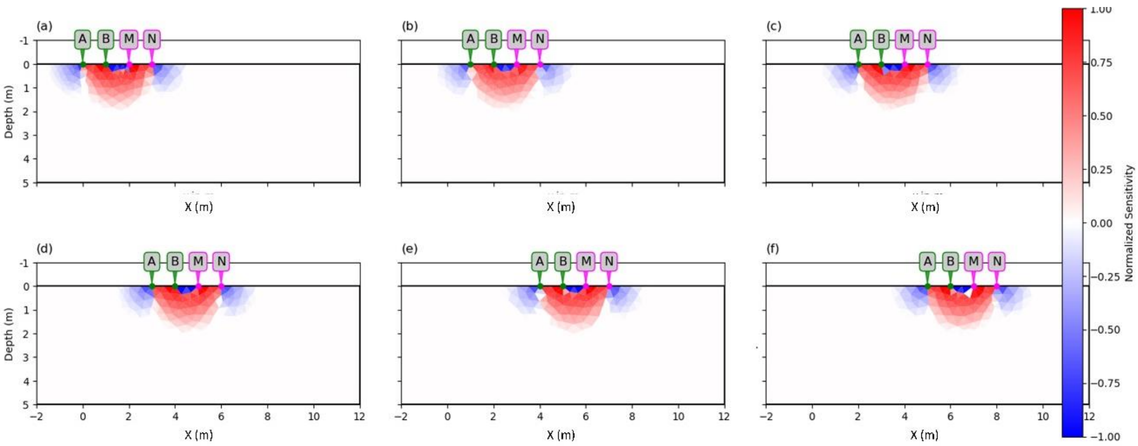

Fig. 4. Plotted Normalized Sensitivity for Wenner-Beta array.

Unique electrode configurations for the Pole-Dipole array, using one current and two potential electrodes, are visualized in Figure 5, presenting six subplots (a–f), each corresponding to a setup.

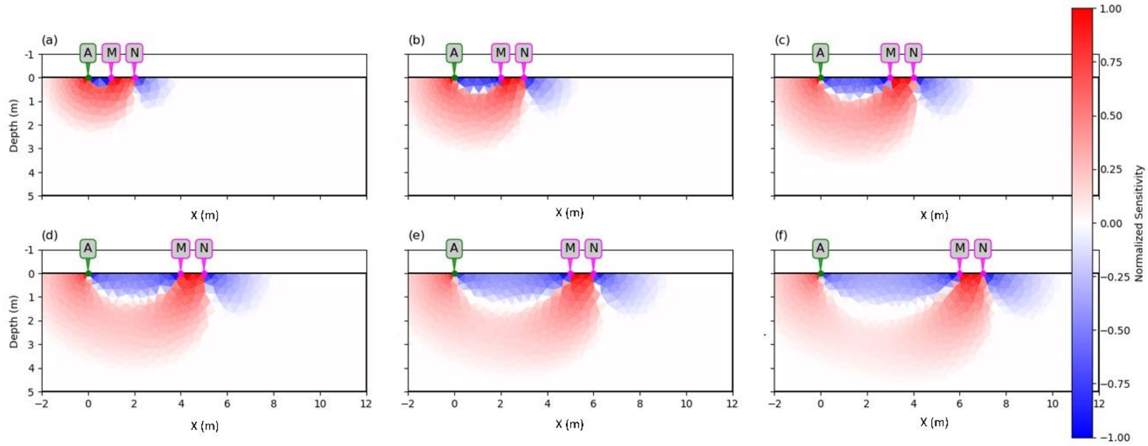

Fig. 5. Plotted Normalized Sensitivity for Pole-Dipole array.

Single current and single potential electrode configurations for the Pole-Pole array are depicted in Figure 6, which displays six subplots (a–f), each showing a distinct sensitivity distribution.

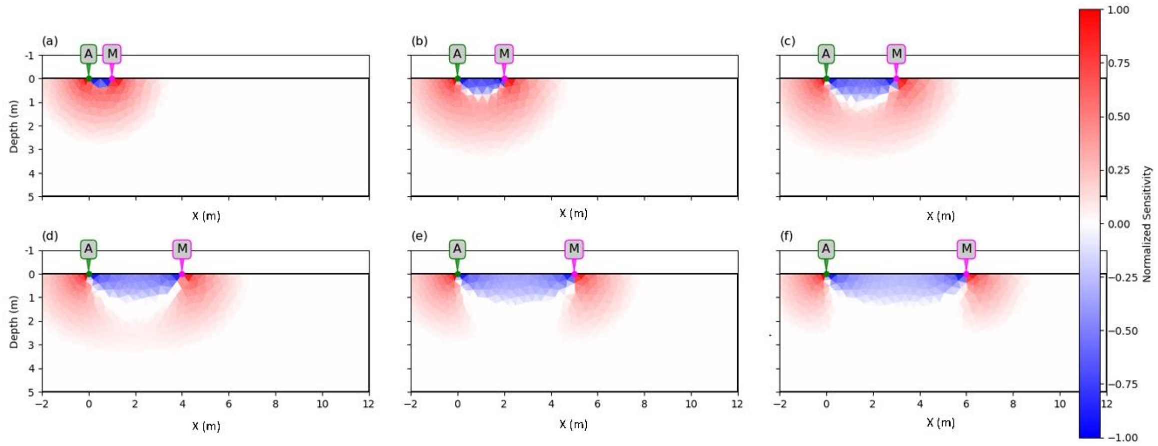

Fig. 6. Plotted Normalized Sensitivity for Pole-Pole array**.**

Apparent resistivity distributions generated for the six electrode arrays—Wenner Alpha, Schlumberger, Dipole-Dipole, Wenner Beta, Pole-Dipole, and Pole-Pole—are illustrated in Figure 7, with six subplots (a–f), each corresponding to the configurations. These subplots highlight variations in apparent resistivity across the synthetic subsurface model, facilitating a comparative analysis of their performance in resolving subsurface electrical properties.

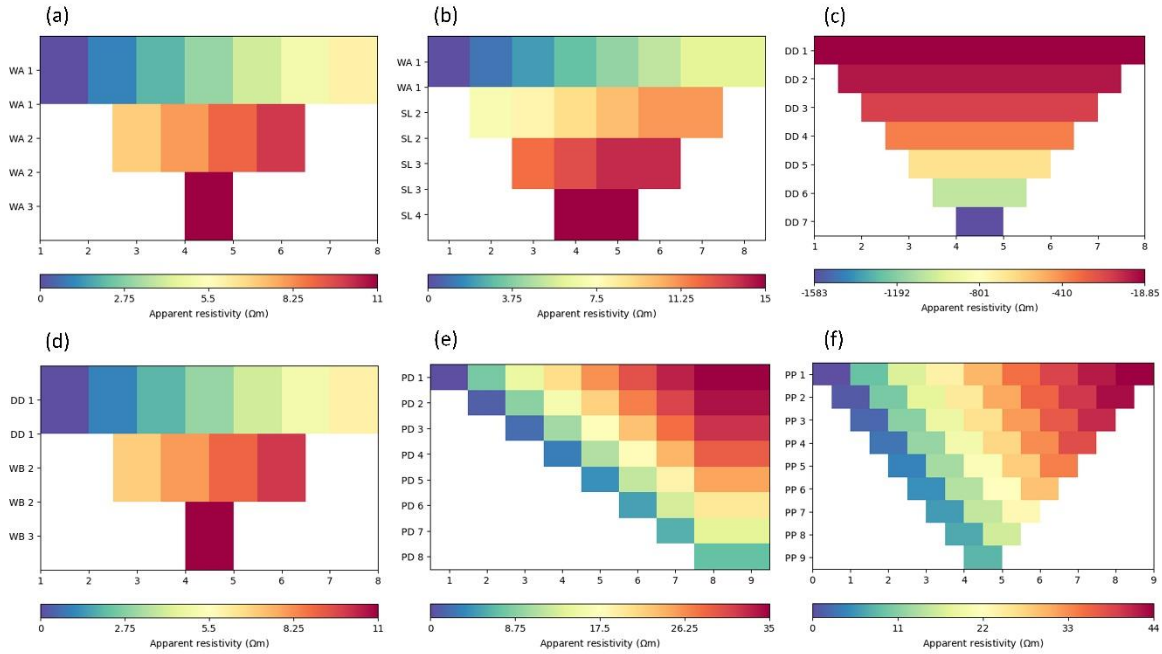

Fig. 7. Plotted Apparent Resistivity Distributions for different arrays.

The synthetic subsurface model used in the geoelectrical simulations is detailed in Figure 8, presented in two subfigures. Subfigure (a) depicts the mesh geometry, comprising a layered subsurface with a rectangular inclusion, discretizing the domain for numerical analysis. Subfigure (b) shows the resistivity distribution, featuring a layered structure with a high-resistivity anomaly embedded within it, highlighting variations in electrical properties across the model.

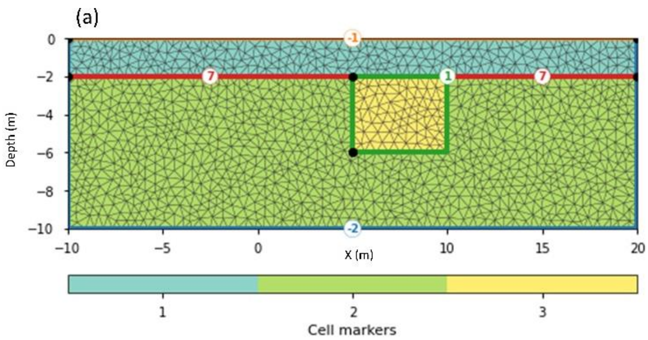

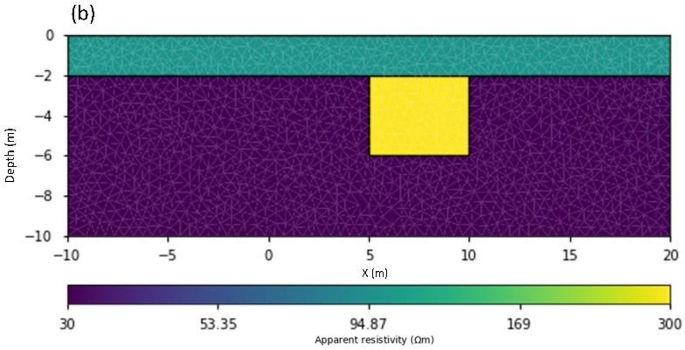

Fig. 8. (a) Primary Synthetic Geometry; (b) Parameterized Synthetic Geometry.

Simulated apparent resistivity for the six electrode arrays—Wenner Alpha, Wenner Beta, Schlumberger, Dipole-Dipole, Pole-Dipole, and Pole-Pole—is visualized in Figure 9, comprising six subplots (a–f), each corresponding to the configurations detailed in Table 1. These subplots enable a comparative assessment of each array's ability to resolve subsurface electrical properties across the synthetic model.

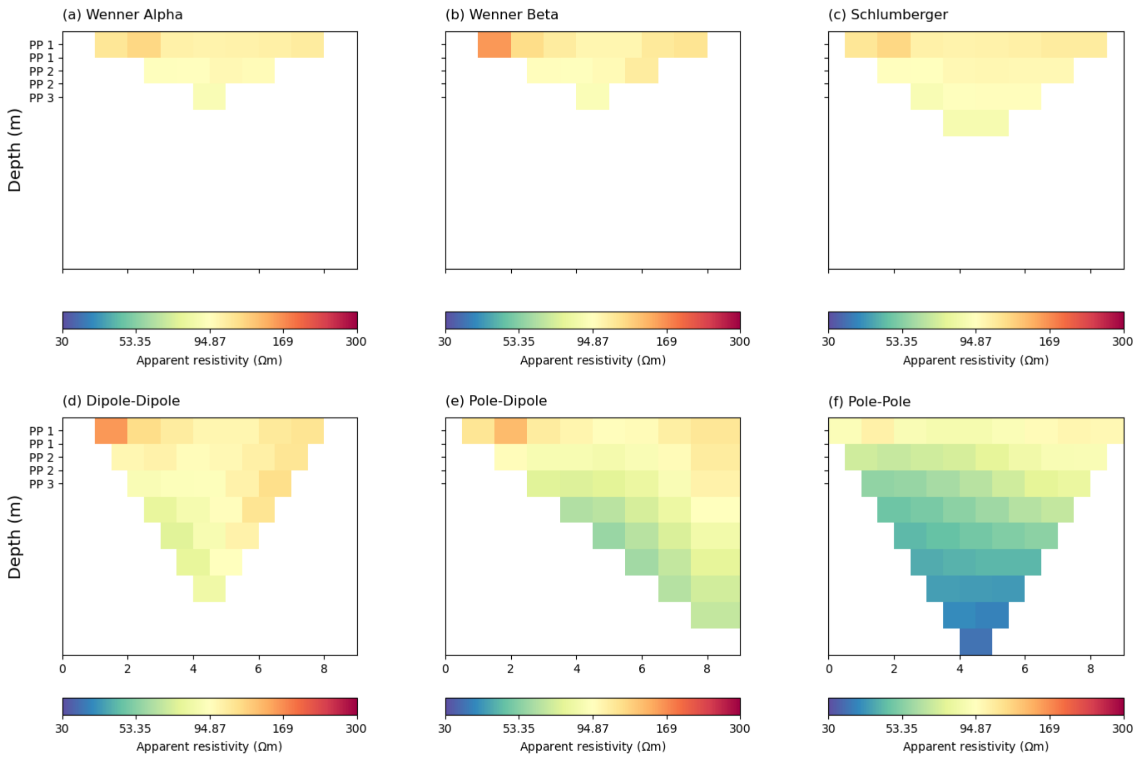

Fig. 9. Observed Apparent Resistivity after Simulation.

Reconstructed subsurface resistivity distributions from inversion for the six electrode arrays—Wenner Alpha, Wenner Beta, Schlumberger, Dipole-Dipole, Pole-Dipole, and Pole-Pole—are shown in Figure 10, with six subplots (a–f), each corresponding to varying configurations. These subplots facilitate a comparative analysis of each array's performance in resolving the synthetic model's electrical properties.

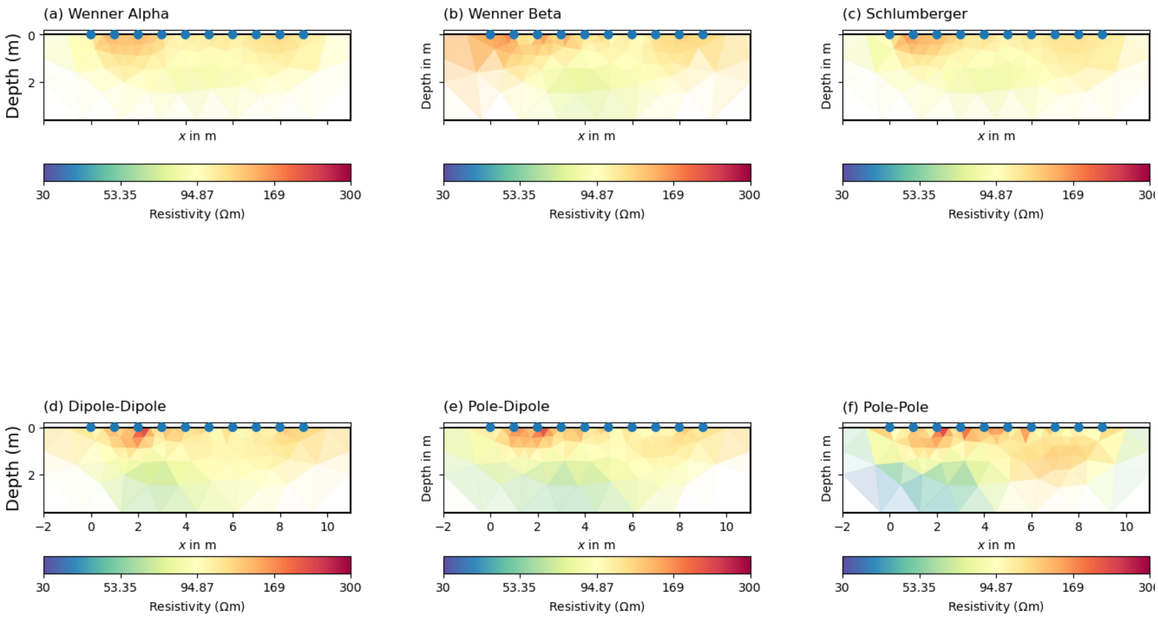

Fig. 10. 2D Models Resulted from Synthetic Electrical Resistivity data Inversion.

5. CONCLUSION

This study evaluated the depth sensitivity and lateral resolution capabilities of six geoelectrical electrode arrays—Wenner Alpha, Wenner Beta, Schlumberger, Dipole-Dipole, Pole-Dipole, and Pole-Pole—through numerical simulations using a synthetic subsurface model with a layered structure and a high-resistivity anomaly. The sensitivity distributions (Figures 1–6) revealed distinct patterns for each array, with smaller electrode separations enhancing near-surface resolution and larger separations improving depth penetration, albeit with potential trade-offs in lateral resolution. The apparent resistivity distributions (Figures 7 and 9) and inverted resistivity models (Figure 10) further highlighted variations in each array's ability to resolve the subsurface electrical properties. Wenner Alpha and Schlumberger arrays demonstrated robust performance for shallow and intermediate depths, while Dipole-Dipole and Pole-Dipole arrays excelled in resolving deeper structures, though with varying lateral detail. Pole-Pole configurations showed the broadest sensitivity but lower resolution, suitable for large-scale surveys. These findings underscore the importance of selecting an appropriate array based on the target depth and resolution requirements, providing valuable guidance for optimizing geoelectrical surveys in diverse subsurface conditions.

REFERENCES

[1] R. J. Whiteley, "Electrode Arrays in Resistivity and I.P. Prospecting: A Review," *Exploration Geophysics*, vol. 4, no. 1, pp. 1–29, Mar. 1973, doi: 10.1071/EG973101.

[2] H. E. Ohaegbuchu, F. C. Anyadiegwu, P. O. Odoh, and F. C. Orji, "Review of top notch electrode arrays for geoelectrical resistivity surveys," *Journal of the Nigerian Society of Physical Sciences*, pp. 147–155, Jan. 2020, doi: 10.46481/jnsps.2019.34.

[3] S. Szalai, A. Novák, and L. Szarka, "Depth of Investigation and Vertical Resolution of Surface Geoelectric Arrays," *J Environ Eng Geophys*, vol. 14, no. 1, pp. 15–23, Mar. 2009, doi: 10.2113/JEEG14.1.15.

[4] T. Dahlin and B. Zhou, "A numerical comparison of 2D resistivity imaging with 10 electrode arrays," *Geophys Prospect*, vol. 52, no. 5, pp. 379–398, Sep. 2004, doi: 10.1111/j.1365-2478.2004.00423.x.

[5] S. Szalai and L. Szarka, "Parameter sensitivity maps of surface geoelectric arrays I. Linear arrays," *Acta Geodaetica et Geophysica Hungarica*, vol. 43, no. 4, pp. 419–437, Dec. 2008, doi: 10.1556/AGeod.43.2008.4.4.

[6] C. C. Okpoli, "Sensitivity and Resolution Capacity of Electrode Configurations," *International Journal of Geophysics*, vol. 2013, pp. 1–12, 2013, doi: 10.1155/2013/608037.

[7] D. J. White, "Two-Dimensional Seismic Refraction Tomography," *Geophys J Int*, vol. 97, no. 2, pp. 223–245, 1989, doi: 10.1111/j.1365-246X.1989.tb00498.x.

[8] R. M. S. White, S. Collins, and M. H. Loke, "Resistivity and IP arrays, optimised for data collection and inversion," *ASEG Extended Abstracts*, vol. 2003, no. 2, pp. 1–4, Aug. 2003, doi: 10.1071/ASEG2003ab182.

[9] C. Rücker, T. Günther, and F. M. Wagner, "pyGIMLi: An open-source library for modelling and inversion in geophysics," *Comput Geosci*, vol. 109, pp. 106–123, Dec. 2017, doi: 10.1016/j.cageo.2017.07.011.

[10] R. Supper *et al.*, "Geoelectrical monitoring: An innovative method to supplement landslide surveillance and early warning," in *Near Surface Geophysics*, EAGE Publishing BV, 2014, pp. 133–150. doi: 10.3997/1873-0604.2013060.